Postprint of: Makarova I., Ryl J., Sun Z., Kurilo I., Górnicka K., Laatikainen M., Repo E., One-step recovery of REE oxalates in electro-leaching of spent NdFeB magnets, Separation and Purification Technology, Vol. 251 (2020), 117362, DOI: 10.1016/j.seppur.2020.117362

One-step recovery of REE oxalates in electro-leaching of spent NdFeB magnets

Irina Makarova[1,], Jacek Ryl[2], Zhi Sun[3], Irina Kurilo[4], Karolina Górnicka[5], Markku Laatikainen[1], Eveliina Repo[1]*

[1] Department of Separation Science, School of Engineering Science, LUT University, Yliopistonkatu 34, FI-53850, Finland

[2] Department of Electrochemistry, Corrosion and Materials Engineering, Gdansk University of Technology, Narutowicza str. 11/12 Gdansk, 80-233, Poland

[3] Beijing Engineering Research Center of Process Pollution Control, Key Laboratory of Green Process and Engineering, Institute of Process Engineering, Chinese Academy of Sciences, Beijing, 100190, China

[4] Department of Analytical and Physical Chemistry, Belarussian State Technological University, Sverdlova 13a str, 220050, Minsk, Republic of Belarus

[5] Department of Solid State Physics, Gdansk University of Technology, ul. Narutowicza, Gdańsk, 11/12, 80-233 Poland

Abstract

Recovery of rare-earth elements (REEs) from spent NdFeB magnets is receiving great attention because of high amount of neodymium and potential risk of environmental pollution. In this study, a novel environment-friendly hydrometallurgical route is proposed for efficient recovery of REEs during electrochemical leaching with sulfuric and oxalic acids. With proper adjustment of the electrolyte composition and operating conditions, effective separation of different elements is observed; a compact layer of REE oxalates in a purity of up to 93% is obtained on the cathode, while iron remains in the solution and as solid residue for further recovery. The mechanisms during the electro-leaching process were subsequently investigated and we propose that cathodic deposition of the REEs is due to electrostatic attraction of the REE-oxalate particles on the cathode. With this finding, selective recovery of REEs from spent magnets can be achieved. This study provides a new insight on electronic waste recycling by implementing principles of electrochemistry.

Keywords: Electrolysis; Rare-earth elements; NdFeB alloy; Adsorption; Oxalic acid

1. Introduction

Over the past decades, consumer demand has led to increasing amounts of electronic and electrical waste, in which large amounts of valuable and precious metals are lost [1, 2]. On

the other hand, some metals like rare-earth elements (REEs) are difficult to mine. They are relatively plentiful in Earth's crust, but because of their geochemical properties, rare-earth elements are typically dispersed and not often found concentrated in rare-earth minerals. As a result, economically exploitable ore deposits are less common [3, 4]. All these factors together with the political aspects concerning with strong quota of REEs from China have made their recycling one of the predominant aims in modern technology [5−10].

Neodymium magnets (NdFeB) are nowadays the strongest magnets that can be used for miniaturization of electronic devices. They are widely used in hybrid cars, turbines, hard drive disks, and headphones. They contain 50−60% of iron, 25−30% of rare-earth elements (mainly neodymium) and around 1% of B. Other elements, such as Al, Ga, Co, Nb, Si, Zr, Ni, Cu, Zn are used as minor additives in order to improve thermal, magnetic or corrosion properties of these magnets [11−15].

All technologies currently available for recycling of spent NdFeB magnets can be divided into hydrometallurgical [16−19] and pyrometallurgical [20, 21] methods. Pyrometallurgical methods demand a lot of energy for melting all the components. Hydrometallurgical technologies are less energy-consuming and can be implemented in different ways. The main steps include demagnetization, mechanical pre-treatment, leaching, and precipitation. The REEs can be precipitated using e.g. oxalic acid. This acid is an effective chelating agent for metal cations and known as very efficient precipitant for REEs (pK_{sp} = 31 – 33) [17, 22, 23]. Other uses for oxalic acid are waste-water treatment [24], biosorbents for removing of heavy metals [25], and fabrication of membranes [26]. Traditionally, used oxalic acid is disposed of as hazardous waste. The reuse of oxalic acid is therefore required from economic and environmental points of view. Van der Hoogerstraete et al. [23] showed a process of recycling of magnets that consumed only oxalic acid, air, and water and produced waste streams such as the leaching residue and the waste from aqueous stripping. Itakura et al. [27] reported that purity of final neodymium oxalate with precipitation by oxalic acid from spent magnets was around 99.8%.

Electrodeposition of REEs from aqueous media is impossible due to their strongly negative reduction potentials [28]. In our previous work, we found that during electro-leaching electrodeposition of iron was accompanied by inclusion of REEs in the cathode deposit [29]. Under certain conditions, deposition of REEs becomes dominant and the presence of oxalic acid in the leaching solution appears to be a crucial factor. To the best of our knowledge, this effect has not been investigated earlier. Aim of this study is to clarify the role of oxalate on the mechanism of direct REE recovery from the electro-leaching solution. For this purpose, number

of analytical methods (SEM, EDX, XRD, XPS) were used to investigate the composition and structure of the cathodic deposit. Moreover, deposition of iron from synthetic solutions and from the actual leach solution was studied by electrochemical analysis.

2. Experimental

2.1 Materials

Spent NdFeB magnets from Webcraft GmbH (Germany) with diameter of 35 mm and thickness of 5 mm were used in all the experiments. The samples were demagnetized at the Curie temperature of 310 °C for 1 hour in an Entech muffle furnace. For proper demagnetization of the working area, the samples were connected by edges. In electrochemical studies NdFeB magnet was used as the anode and copper plate as the cathode (0.2 dm^2). Anodes were mechanically polished with #500, #900, #1200 and #2000 emery paper, then with Al_2O_3 suspension, and finally degreased with ethanol.

Sulfuric acid (Sigma-Aldrich, 98%) or mixture of sulfuric and oxalic acid (Sigma-Aldrich, >97.5%) were used as leaching agent. Solutions were prepared by diluting with MilliQ water (Merck Millipore Q-POD) to the desired concentrations.

2.2 Electrochemical leaching

All leaching experiments were carried out at 22 ± 1°C in a 150 mL glass beaker in galvanostatic mode using a PS 3005 power supply. In the electrochemical leaching experiments with the polished magnets, anode current density was i = 50 A/dm^2. The temperature of the electrolyte was controlled by a water bath (RK8 CS, Lauda). The pH and conductivity of the leach solutions was monitored using standard procedures (Radiometer PHM 240 pH/ion pH meter and Knick 703 conductivity meter).

Concentration of sulfuric and oxalic acids was 0.5 mol/L and 0.05 mol/L, respectively. Solid to liquid ratio was kept at 0.05 dm^2 of NdFeB alloy surface per 80 mL of solution and magnetic stirring speed was ω = 400 rpm. Maximum duration of electro-leaching was 2 h. The magnet samples and copper cathodes were weighted before and after leaching using Mettler AC 88 analytical scale.

2.3 Electrochemical measurements

Electrochemical measurements were carried out in a three-electrode cell with saturated silver/silver chloride as reference electrode, platinum wire as counter electrode, and a copper substrate (exposed surface area 1 cm^2) as working electrode using an Autolab PGSTAT 302N

potentiostat-galvanostat (Methrom). Prior to the experiments, working electrodes were immersed in the electrolyte for 30 min. Potentiodynamic polarization was carried out at a 5 mV/s sweep rate in cathodic direction. The temperature was controlled by a water jacket and a thermostat. Cathodic polarization curves were obtained for a leach solution obtained after 1hour and for synthetic solutions of ferrous and ferric sulfate in the presence and absence of oxalic acid and/or Nd sulfate. In the synthetic solutions, c_{Fe} = 10 g/L and c_{Nd} = 2 g/L.

2.4 Characterization methods

Surface morphology and composition were measured using Hitachi SU3500 scanning electron microscopy (SEM) equipped with an energy dispersive X-ray (EDX) unit. The chemical composition and crystal structure of the cathode and anode before and after electro-leaching were further ascertained using X-ray diffraction (XRD) (Bruker D8 Advance) with Cu Kα irradiation. The 2θ range was 10 – 70° and step size 0.02 °/s.

Cathode deposits, which were obtained after electro-leaching for 45, 60, 90 and 120 min in the mixture of sulfuric and oxalic acids, were washed thoroughly with water, removed from copper substrate and digested. The filtered solution was analyzed with inductively coupled plasma mass spectroscopy (ICP-MS, Agilent 7900) in a mixture of 1% HNO_3 and 1% HCl (Ultrapure, Merck). Relative standard deviation of all ICP measurements were less than 3.6%.

X-ray photoelectron spectroscopy (XPS) was used for the characterization of cathodic deposits after 1 and 2 hours of electro-leaching. The samples were cleaned in deionized water for 10 min and dried. No other treatment was implemented in order not to compromise the subtle chemical changes on the surface. Spectra were recorded in the Fe2p, Nd5d, B1s, C1s and O1s binding energy (BE) range for each sample to verify their surface chemistry. The measurements were carried out using Escalab 250Xi multispectroscope (ThermoFisher Scientific) equipped with Al Kα monochromatic X-Ray source and spot diameter of 0.65 mm. Applied pass energy was 10 eV and the energy step size 0.1 eV. Charge compensation was controlled through low-energy electron and low-energy Ar+ ions emission using the flood gun (emission current 0.15 mA). The XPS depth of analysis is approximately 5 nm.

ζ-potential of neodymium oxalate particles was measured by an electro-kinetic analyzer (SurPASS, Anton Paar) using 1 mM KCl solution as the background electrolyte. Neodymium oxalate particles were obtained by mixing $Nd_2(SO_4)_3$ (Sigma-Aldrich) and oxalic acid in aqueous solution at a molar ratio of 1:3. The precipitate was thoroughly washed, filtered and packed in a cylindric cell. The pH range was from 5 to 2 and a HCl solution was used in pH adjustment.

2.5 Efficiency of electro-leaching

For assessment of the electrodeposition conditions, current efficiency (ε) was calculated. In some cases, ε was more than 100% due to the active dissolution and substantial contribution of chemical leaching. Energy consumption W (in kWh/kg of NdFeB magnet) was calculated from Eq. (1), where U is the average cell voltage on cell (V) and ε is the current efficiency. For iron, $q_{\mathrm{Fe}} = M_{\mathrm{Fe}}/z_{\mathrm{Fe}}F = 1.05$ g/(Ah) and for neodymium $q_{\mathrm{Nd}} = 1.79$ g/(Ah), where z is the ion charge and F the Faraday constant.

$$q_{alloy} = \frac{U}{q_{alloy}\varepsilon}$$
$$q_{alloy} = \frac{q_{Fe}q_{Nd}}{q_{Fe}w_{Fe} + q_{Nd}w_{Nd}} \qquad (1)$$

Purity of cathodic deposit, P, and REE yield, Y, were calculated from Eqs (2) and (3), where m_{REE} and m_{other} are weights of rare-earths and other metals in the deposit. The superscripts dep and sol refer to the deposit and solution, respectively.

$$P = \frac{m_{REE}^{dep}}{m_{REE}^{dep} + m_{others}^{dep}} \cdot 100\% \qquad (2)$$

$$Y = \frac{m_{REE}^{dep}}{m_{REE}^{dep} + m_{REE}^{sol}} \cdot 100\% \qquad (3)$$

All experiments were done in triplicate to ensure statistical reliability of the results.

3 Results and discussion

3.1 Electro-leaching of spent NdFeB magnet

Electro-leaching of spent NdFeB magnet was studied using 0.5 M H_2SO_4 and a mixture of 0.5 M H_2SO_4 and 0.05 M $H_2C_2O_4$. The results have been reported previously [29] and only those obtained at high current density of 50 A/dm^2 and in the presence of oxalic acid are shown in Fig. 1. The data obtained without electricity are shown for the sake of comparison.

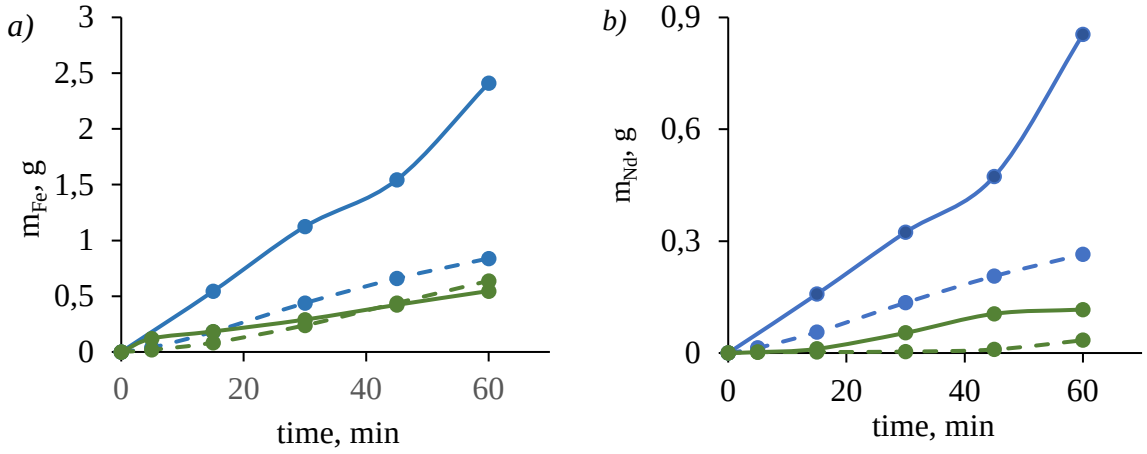

Figure 1. Amount of iron (*a*) and neodymium (*b*) leached from NdFeB magnet waste in 0.5 M H_2SO_4 (blue) and in 0.5 M H_2SO_4 + 0.05 M $H_2C_2O_4$ (green). i = 0 A/dm^2 (solid lines), 50 A/dm^2 (dashed lines)

Under these rather extreme conditions, dissolution of Fe (Fig. 1*a*) and Nd (Fig. 1*b*) decreased probably due to intensification of competitive processes like oxygen evolution and passivation of magnet surface by oxidation. It is important to note that the values in Fig. 1 were calculated from the solution concentrations and they do not include precipitated species. This is especially true for Nd and other REEs because of formation of sparingly soluble oxalates [29]. As a result, the solution concentration of Nd was only a third of the value observed without oxalic acid after 1 hour of electro-leaching.

The focus of this study is on the cathodic deposition taking place during electro-leaching. The experimental data showing the amount and composition of the deposit are given in Table 1. The REE yield and purity were calculated using Eqs (2) and (3) and the results are shown in Fig. 2.

Table 1. Content of main components in the cathodic deposit and in the solution during electro-leaching. W is the energy consumption. T = 22 °C, i=50 A/dm^2, ω = 400 rpm)

Time, min	Δm_{anode}, g	$\Delta m_{cathode}$, g	Concentration of metals in deposit, mg/g				Weight in deposit, g		Weight in solution, g		U_{cell}, V	W, kWh/kg
			Fe	Pr	Nd	Gd	Fe	Nd	Fe	Nd		
0	–	–	–	–	–	–	–	–	–	–	3.2	–
10	0.267 ±0.008	–	–	–	–	–	–	–	–	–	7.6	27.08
20	0.473 ±0.015	0.020 ±0.003	–	–	–	–	–	–	–	–	7.6	15.57
30	0.558 ±0.031	0.027 ±0.004	–	–	–	–	–	–	0.290	0.054	7.7	13.41
45	0.984 ±0.206	0.200 ±0.051	241.8 ± 43.8	46.0 ± 5.5	166.5 ± 25.1	41.6 ± 6.6	0.004	0.082	0.420	0.105	8.0	7.72
60	1.047 ±0.153	0.231 ±0.027	34.3 ± 10.9	69.3 ± 0.5	247.9 ± 1.9	60.1 ± 1.8	0.037	0.264	0.550	0.112	8.7	7.44
90	1.507 ±0.111	0.412 ±0.061	35.0 ± 9.2	68.2 ± 0.2	247.5 ± 1.9	60.7 ± 1.1	0.034	0.248	2.195	0.442	11.9	6.90
120	2.735 ±0.009	0.686 ±0.130	13.2 ± 0.06	74.2 ± 1.7	254.0± 16.3	61.0 ± 5.1	0.216	0.201	2.449	0.765	18.6	5.80

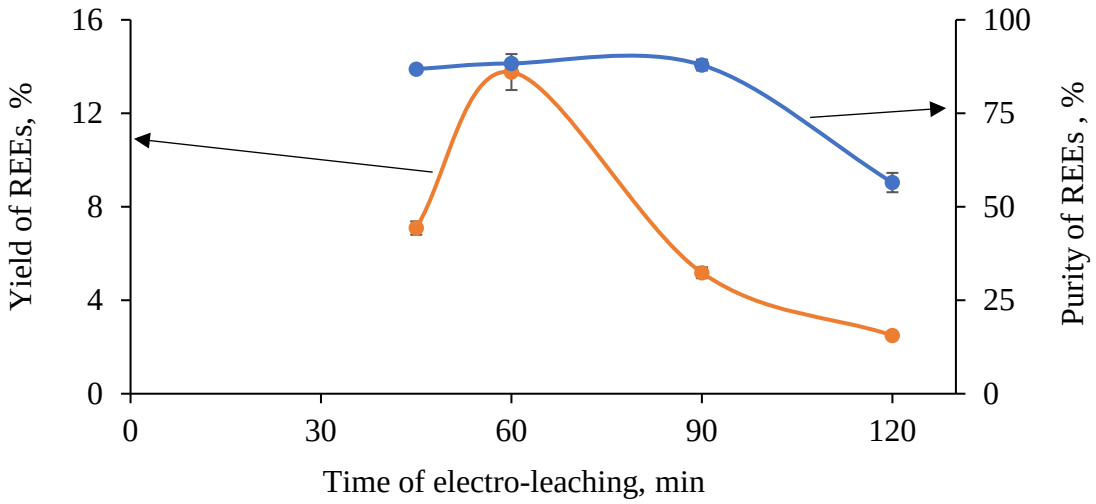

Figure 2. Yield and purity of REEs in cathodic deposit during electro-leaching of spent NdFeB magnet in a mixture of 0.5 M H_2SO_4 and 0.05 M $H_2C_2O_4$ at 50 A/dm^2.

As shown in Table 1, electrochemical leaching for 2 hours in a mixture of 0.5 M H_2SO_4 and 0.05 M $H_2C_2O_4$ at 50 A/dm^2 dissolved 2.74 g of the NdFeB magnet and 0.69 g were deposited on the cathode. About 0.39 g of Nd, Pr and Gd was found in the cathodic deposit and mass balance calculations show that they are in the form of oxalate ($REE_2(C_2O_4)_3 \cdot 10H_2O$).

After about 60 min, mainly REE complexes deposited on the cathode and the purity on metal basis was 86−88% (Fig. 2). Further leaching beyond 90 min led to decrease in purity, probably because exhaustion of oxalic acid in the solution and subsequent increase of iron reduction. Offered method allows to obtain around 70% of total amount of Nd at cathode.

In order to explore the leaching mechanism, cell voltage as well as anode and cathode potentials were monitored. The results are shown in Fig. 3 and the electrode potentials are given on the SHE scale. Moreover, bulk pH and conductivity were measured after 1 hour of electrolysis and the results are shown in Fig. 1S (supplementary material).

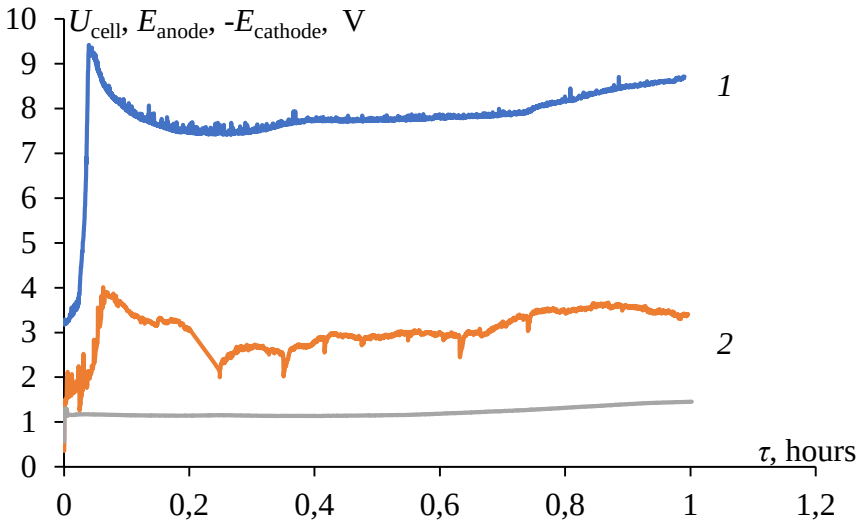

Figure 3. Variation of cell voltage (*1*), anode potential (*2*) and cathode potential (*3*) during electro-leaching of spent NdFeB magnet in 0.5 M H_2SO_4 + 0.05 M $H_2C_2O_4$. T = 22 °C, ω = 400 rpm, i = 50 A/dm^2.

Open circuit potential of anode was 0.56 V and the sharp increase during the first 3 minutes can be explained by selective dissolution of the more reactive components including Nd and other REEs (Eq. (4)) (in the following equations, E^0 stands for the standard reduction potential on the SHE scale). Subsequent decrease of the anode potential indicates more uniform dissolution of iron that is the more electronegative component in the magnet (Eqs (5)-(7)).

$$Nd^{3+}(aq) + 3e^- \rightleftharpoons Nd(s) \qquad E° = -2.32\ V \qquad (4)$$

$$Fe^{2+}(aq) + 2e^- \rightleftharpoons Fe(s) \qquad E° = -0.44\ V \qquad (5)$$

$$Fe^{3+}(aq) + 3e^- \rightleftharpoons Fe(s) \qquad E° = -0.037\ V \qquad (6)$$

$$Fe^{3+}(aq) + e^- \rightleftharpoons Fe^{2+}(aq) \qquad E° = 0.77\ V \qquad (7)$$

In the presence of oxalic acid, anodic oxidation can also proceed according to Eqs (8)−(10) [30−32] that result in precipitation of Nd and other REEs and complexation of ferrous and ferric ions.

$$2Nd(s) + 3C_2O_4^{2-}(aq) + 10H_2O \rightleftharpoons Nd_2(C_2O_4)_3 \cdot 10H_2O(s) + 6e^- \quad (8)$$

$$Fe + nHC_2O_4^-(aq) \rightleftharpoons [Fe(C_2O_4)_n]^{2-2n}(aq) + nH^+(aq) + ne^- \quad (9)$$

$$Fe + nHC_2O_4^-(aq) \rightleftharpoons [Fe(C_2O_4)_n]^{3-3n}(aq) + nH^+(aq) + ne^- \quad (10)$$

After the initial period, the anode potential remains more or less constant in the range of 2.5−3.5 V (Fig. 3) and may induce oxidation of iron [30−32]. Moreover, active evolution of oxygen due to Eq. (11) was observed.

$$2H_2O \rightleftharpoons 4H^+(aq) + O_2(g) + 4e^- \qquad E° = 1.23\ V \quad (11)$$

During electro-leaching at 50 A/dm^2, solution pH initially increased due to consumption of the protons in the leaching reactions and because of hydrogen evolution at the cathode (Eq. (12). In principle, hydrogen can be also formed in the reaction between the acid and the magnet but because of the high anode potential, this reaction is effectively suppressed.

$$2H^+(aq) + 2e^- \rightarrow H_2(g) \qquad E° = 0.00\ V \quad (12)$$

At later stages pH decreased probably because of the intensification of the oxygen evolution (Eq. 11). Solution conductivity decreased during electro-leaching as the hydrogen ions were replaced by less conductive components released from the magnet [33].

Calculated energy consumptions and amount of Fe and REEs in cathodic deposit and in a solution during 2 hours of electrolysis obtained from ICP analysis are presented in Table 1 and Fig 2S. During increasing of electrolysis time from 10 minutes to 2 hours average energy consumptions decreased from 27.1 to 5.80 kWh/kg.

In summary, anodic dissolution at high current densities and in the presence of oxalic acid takes place under highly oxidative conditions and the main products are ferric oxalate complexes and insoluble REE oxalates. Composition of the leached magnet residue is discussed in next Section.

3.2 Effect of electro-leaching on the NdFeB magnets

Influence of etching and electrochemical leaching on the polished NdFeB magnet is illustrated in Figure 4.

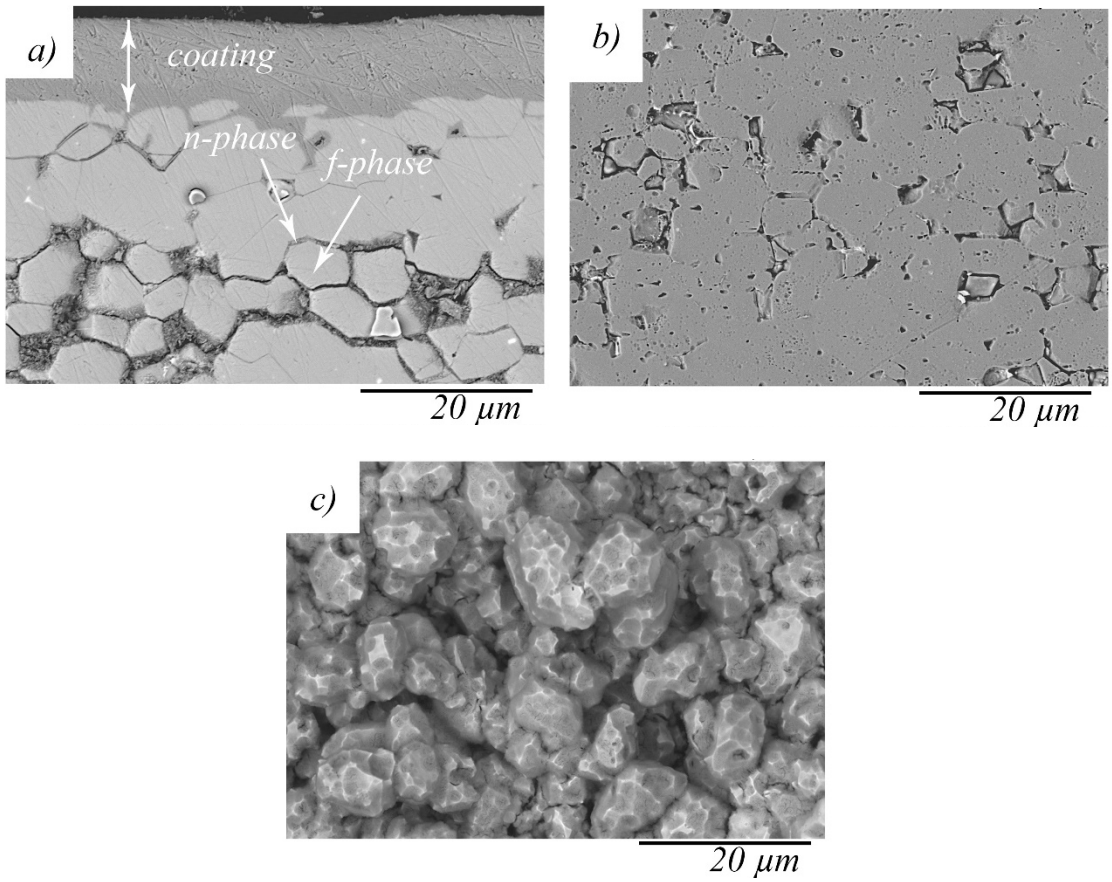

Figure 4. SEM images of the spent NdFeB magnet surface initially (*a*), after 10 s etching in 1 M HNO_3 (*b*) and after 1 h electrochemical leaching in a mixture of 0.5 M H_2SO_4 and 0.05 M $H_2C_2O_4$ at i=50 A/dm^2 *(c)*

Commercial NdFeB magnets are coated with a Ni-Cu-Ni layer for the anticorrosion properties and the main structure consists of the ferromagnetic matrix (f-phase) and Nd-rich interstitial phase (n-phase) [29, 34] as shown in Fig. 4*a*. Before the leaching experiments, magnets were demagnetized, coating was chemicaly removed by 1 M nitric acid and surface was mechanically polished. Etching in nitric acid (Fig. 4*b*) led to some dissolution because of high reactivity of the n-phase and formation of galvanic pairs between n- and f-phases.

In our previous work [29], we showed that application of electric current does not significantly influence the surface characteristics during dissolution both in sulfuric acid solution and in a mixture of sulfuric and oxalic acids. However, during electro-leaching at high current densities and with oxalic acid, magnet surface was more extensively oxidated and

formation of insoluble products may lead to passivation of the magnet surface. When the anode current density was increased from 0 to 50 A/dm^2, the oxygen content more than doubled from 7.2 to 14.8 wt-%. (Table 2). Moreover, even protruding edges began to dissolve under these conditions and the Fe-rich nodules dominate in the residue (Fig. 4*c*). Regardless of the leaching conditions, the XRD pattern of the leached NdFeB magnet showed predominance of the $Nd_2Fe_{14}B$ phase [29] (Fig. 3S in supplementary material). As expected, peaks that are characteristic to ferric oxides are also present in accordance with Table 1 and with the discussion in the previous Section.

Table 2. Elemental composition of spent NdFeB magnet surface after leaching under various conditions.

Leaching solution	Current density, A/dm^2	Elemental composition, wt%									
		C	O	Al	S	Fe	Cu	Zr	Pr	Nd	Gd
0.5 M H_2SO_4	0	3.2	7.2	0.3	–	53.8	6.0	1.6	5.6	18.1	4.2
	10	3.2	8.1	0.2	0.3	56.2	3.9	1.3	4.4	18.4	3.8
	50	2.6	14.8	0.3	0.9	56.7	–	–	4.2	16.7	3.8
+ 0.05 M $H_2C_2O_4$	50	3.7	23.5	0.2	2.1	47.9	–	0.9	3.8	14.9	2.9

3.3 Characterization of cathodic deposit

During the electrochemical leaching of the spent NdFeB magnet, compact and uniform cathodic deposit was observed only in a mixture 0.5 M H_2SO_4 and 0.05 M $H_2C_2O_4$ at i = 50 A/dm^2. SEM images of the coating are shown in Fig. 5. Under other conditions no deposit was observed.

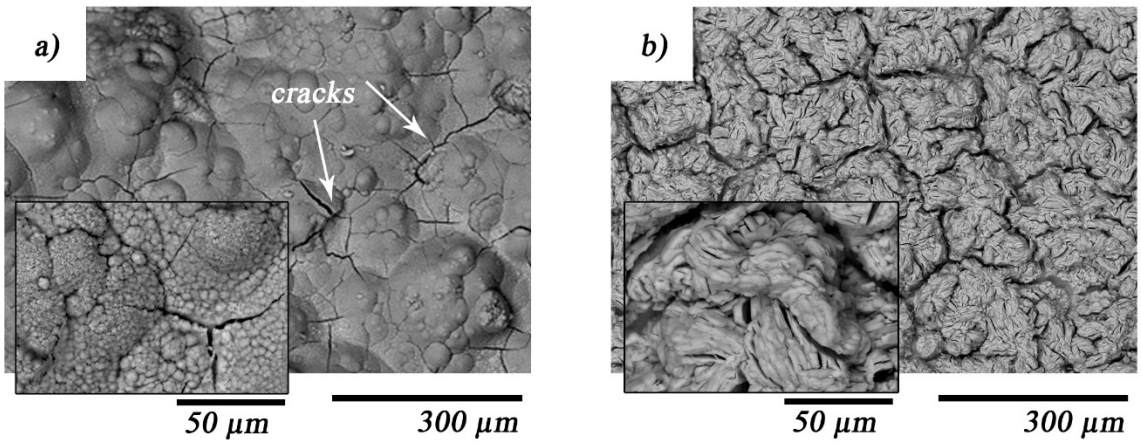

Figure 5. SEM images of the cathode deposit obtained during anodic dissolution of NdFeB in a mixture of 0.5 M H_2SO_4 and 0.05 M $H_2C_2O_4$ at 50 A/dm^2. Time of electro-leaching was 1 hour (*a*) and 2 hours (*b*).

After 1 h, the surface of the cathodic deposit had a lot of cracks (Fig. 5*a*) due to active evolution of hydrogen but after 2 h, a fibrous structure was observed. EDX analysis (Table 2S, Supplementary material) revealed that composition of the sediment changed markedly during electro-leaching. After 1 h leaching, the copper substrate was mainly coated by metallic iron (75.4 wt-%) with some incorporation of REEs. Iron content reduced significantly to about 1 wt-% after 1.5 h suggesting that Fe^{2+} reduction was displaced by other reactions. During further leaching (1.5−2 h), the sediment was mainly composed of carbon-containing compounds of Nd and other REEs (Pr, Gd). The XRD patterns (Fig. 6) shows that the main phases deposited on the cathode after 2 h were $Nd_2(C_2O_4)_3 \cdot 10H_2O$ and Fe.

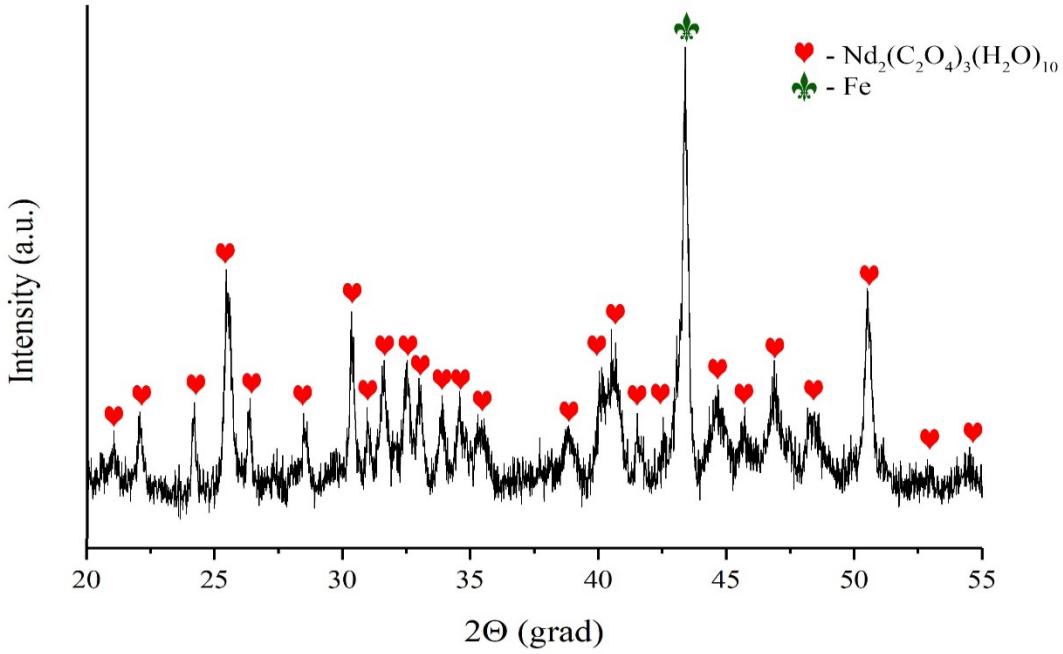

Figure 6. XRD patterns of the cathode deposit after 2 hours of electro-leaching of spent NdFeB magnet. Leaching was done in a mixture of 0.5 M H_2SO_4 and 0.05 M $H_2C_2O_4$ at 50 A/dm^2

As shown in Fig. 7 for Fe and Nd and in Fig. 5S (supplementary material) for other elements, the distribution in the sediment is quite homogeneous. It is visible that after 1 hour of electrolysis matrix consist mainly from iron with dots of neodymium (Fig. 8*a*). Further continuation of electrolysis leads to de-ironing of surface and it covered by full and compact neodymium oxalate layer.

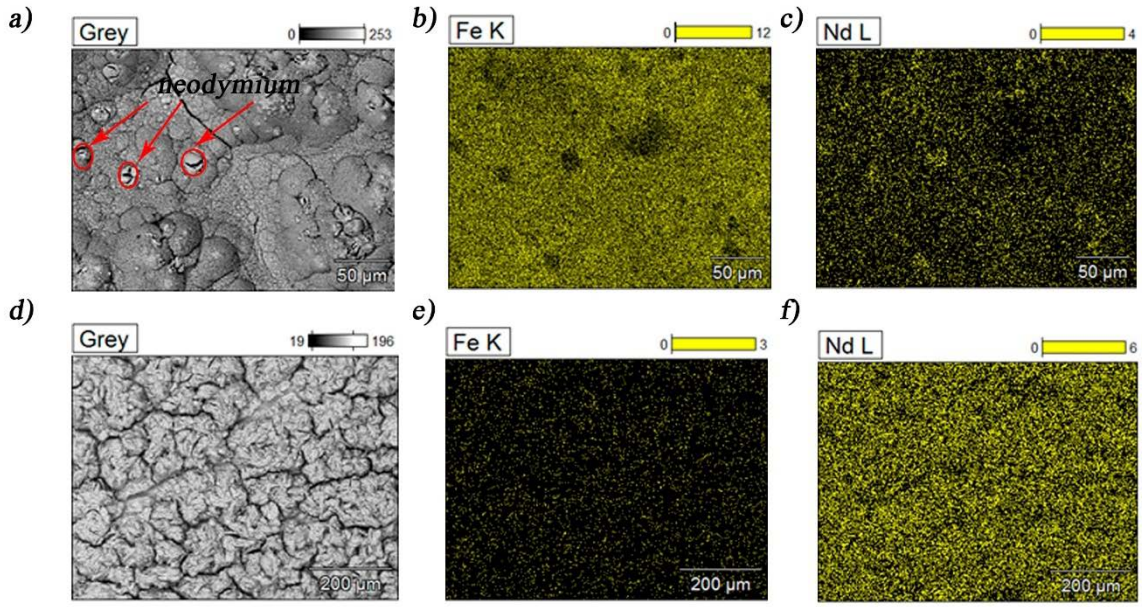

Figure 7. High-resolution EDX mapping of the cathode deposit after electro-leaching for 1 h (*a*–*c*) and 2 h (*d*–*f*). *i*= 50 A/dm^2.

Next, high-resolution XPS analysis was used to get a more detailed surface composition of the cathodic deposit. The raw spectra were deconvoluted into main components and the results are shown in Fig. 8.

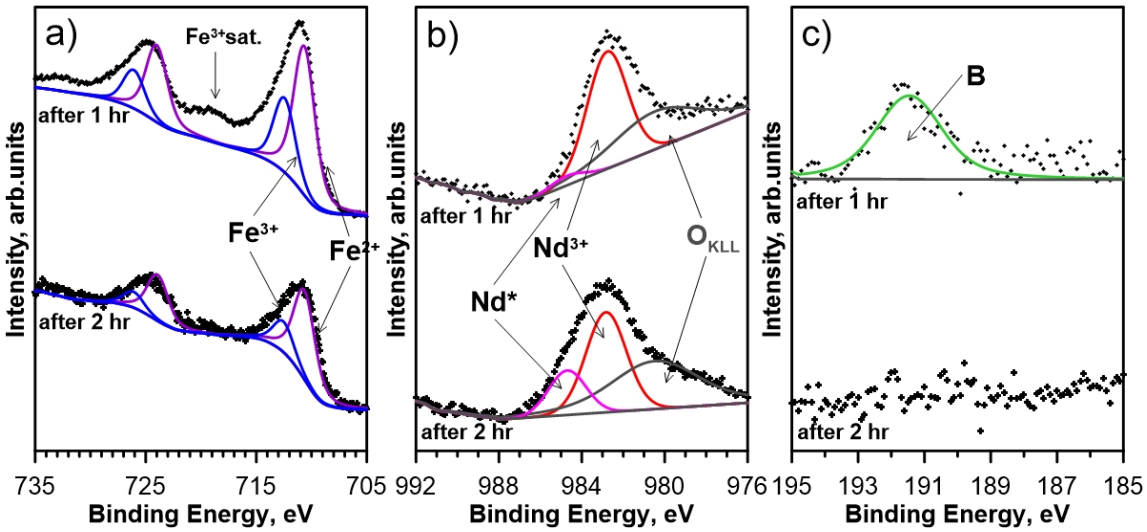

Figure 8. High-resolution XPS spectra registered in the binding energy range of a) Fe 2p; b) Nd $3d_{5/2}$; and c) B 1s for the cathodic deposit obtained after 1 hour and 2 hours.

Iron is present in two chemical states, with peaks centered at a binding energy of 710.6 ± 0.1 eV and 712.4 ± 0.1 eV (Fig. 8a), which correspond to Fe^{2+} and Fe^{3+} species, respectively. The Fe^{2+}/Fe^{3+} ratio slightly increases with time; from 2.1 after 1 hour to 3.0 after 2 hours of electrolysis, which is understandable given the occurrence of reduction processes at the cathode. Based on the obtained results iron is most probably present as a mixture of FeO and Fe_3O_4 [35−38].

The Nd $3d_{5/2}$ spectra (Fig. 8b) show a peak corresponding to Nd_2O_3 and a satellite peak observed at about 10 eV higher. The latter most probably represents Nd bound with oxalic acid. Moreover, the XPS analysis indicated absence of Pr on the surface of cathodic sediment, while plenty of it was found inside the deposit by EDX and ICP analyses. The reason for differences between EDS and XPS results is the low depth of analysis of the latter technique, which is only up to 5 nm. It should be noticed that the surface of both sediments consists mostly of hydroxide and carbon-containing species (oxalates).

Another difference in these two analyses is seen in the case of boron. The EDX technique is not sensitive enough to detect boron due to very small kinetic energy of boron Kα signal, determined by low atomic mass of this element. On the other hand, the XPS B_{1s} spectra reveals presence of this element (Fig. 9c). Established boron peak is centered at a binding energy of (191.5 ± 0.1) eV after 1 h of electrolysis and corresponds to B_2O_3 [39, 40]. Increasing time of electrolysis to 2 h leads to disappearing of boron from coating surface.

In view of Eq. (4), deposition of Nd on the cathode is quite surprising and therefore other experiments were attempted to find the deposition mechanism. Electrochemical measurements were made to clarify reduction of iron from different solutions. Polarization curves for synthetic ferrous and ferric sulfate solutions and from a solution obtained after 1 h electro-leaching are depicted in Figure 9.

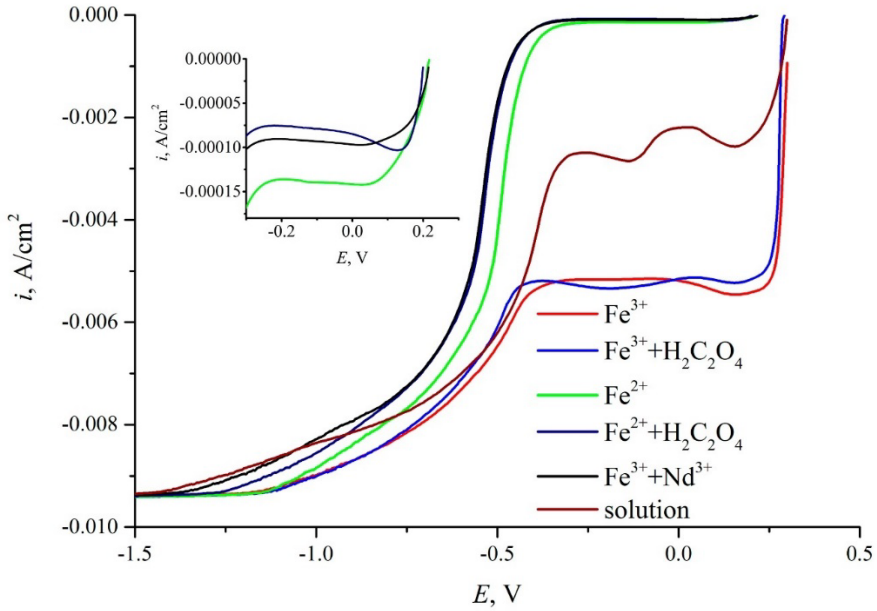

Figure 9. Linear polarization curves of synthetic solutions (c_{Fe} = 10 g/L and c_{Nd} = 2 g/L) and a leaching solution obtained after 1 h electro-leaching. Insert shows the initial part of Fe^{2+} reduction curves.

Reduction of Fe^{2+} ions (Eq. (4)) began at $E = -0.32$ V and addition of oxalic acid shifted it to more negative values ($E = -0.39$ V) because of complexation with oxalate. Addition of Nd^{3+} did not significantly affect the reduction overpotential and the curve matches with that of the solution that contained only Fe^{2+} and oxalic acid. At a current density of 0.006 A/cm^2 starts evolution of hydrogen. As expected, reduction of Fe^{3+} ions takes place stepwise according to Eqs (6) and (4), and the polarization curves show two separate waves. Reduction began at $E = -0.04$ V and around $E=-0.5$ V, it is accompanied by evolution of hydrogen (Eq. (11)). The presence of oxalic acid again shifted Fe^{2+} reduction wave to more negative potentials, while effect on reduction of Fe^{3+} was very small.

The polarization curve of the leach solution suggests that iron is present mainly as Fe^{3+}. Iron concentration in the leach solution was 8.6 g/L. Moreover, the wave representing hydrogen evolution was substantially stronger due to higher acid concentration.

3.4 Mechanism of REE recovery on the cathode

On the basis of the above data, a mechanism for electroleaching/electrodeposition was proposed and it is schematically depicted in Fig. 10. As the anodic process was explained in detail in our previous work [29], this scheme focuses on the cathodic process.

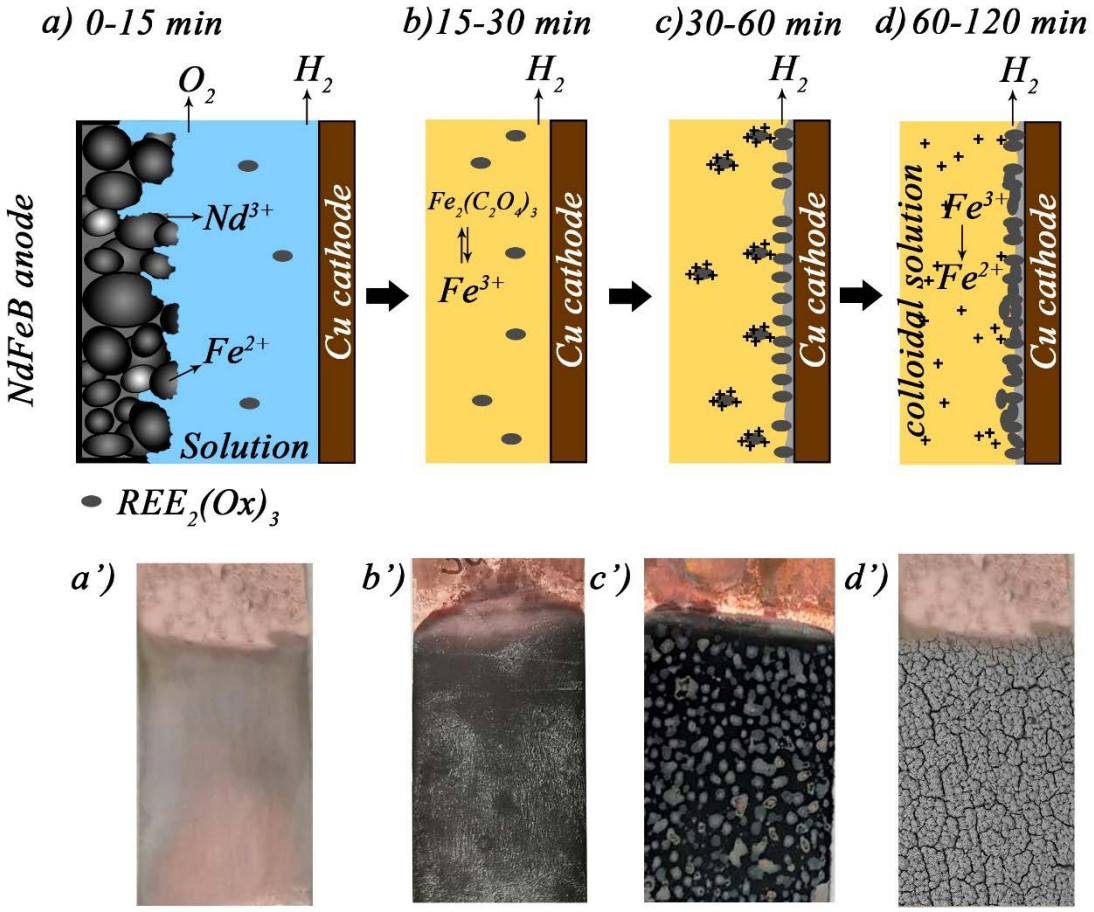

Figure 10. Proposed mechanism for electro-leaching of spent NdFeB magnets in a mixture of 0.5 M H_2SO_4 and 0.05 M $H_2C_2O_4$ (*a*–*d*) and appearance of the cathode (*a*' – *d*').

During the first half an hour, concentration of metal ions in the electrolyte was quite low (Fig. 1) and no reduction of iron on the cathode took place. However, presence of oxalic acid allowed to form fine REE oxalate ($REE_2(C_2O_4)_3 \cdot xH_2O$) particles (Fig. 11*a*, 11*b*). The solubility product of REE oxalates is very low, pK_{sp} = 31 – 33, and the dissolved metals are effectively precipitated. The particles were characterised using XRD and zeta-potential measurements. As shown in Figs 5S and 6S(in supplementary material), the XRD peaks can be assigned to REE oxalates (Nd-oxalate used here as the model compound) and the particles are positively charged under acidic conditions. We thus propose that the positively charged REE oxalate particles moving with the liquid flow collide and stick on the cathode thus forming the REE-rich deposit. It is not yet clear why this process displaces iron reduction and inhibits Fe deposition.

After 15 minutes, the color of the solution became strongly yellow indicating the oxidation of iron from Fe^{2+} to Fe^{3+} (Eq. 3) and formation of soluble oxalate complexes of

iron (III). After 1 hour, pH in vinicity during electrolysis significantly changing and iron stops to deposite on cathode. Iron (Fe^{3+}) ions are a transporter of oxalate ions during this time, they are destroying and releasying additional amount of oxalate ions (eq. 13), that formed complexes with REEs $Nd_2(C_2O_4)_3 \cdot xH_2O$ (eq. 15 and 16):

$$FeC_2O_4^{+} + H_2 + e^{-} \rightarrow Fe^{2+} + C_2O_4^{2-} + 2H^{+} \quad (13)$$

And it also takes place partial reduction of Fe^{3+} to Fe^{2+} by evoluted hydrogen (eq. 14), but oxalate of neodymium most probably due to electrostatic adsorption, as it was established that it has positive charge in acidic media (Fig. 7S) [41, 42], starts to diffuse to the cathode surface and discharge to forming coating (eq. 15 and 16).

$$2Fe^{3+} + H_2 \rightarrow 2Fe^{2+} + 2H^{+} \quad (14)$$

$$2Nd^{3+} + 3H_2C_2O_4 + xH_2O + 6e^{-} \rightarrow Nd_2(C_2O_4)_3 \cdot xH_2O + 3H_2 \quad (15)$$

$$2[NdC_2O_4]^{+} + H_2C_2O_4 + 10.5H_2O + 2e^{-} \rightarrow Nd_2(C_2O_4)_3 \cdot 10.5H_2O + H_2 \quad (16)$$

4 Conclusions

In this study, a proof-of-principle is given for a process, in which the rare-earths metals are recovered from the NdFeB magnet in high purity by using only demagnetization, etching, and electro-leaching steps. The process scheme is outlined below. Purity of final REE-oxalate product is 91−93% (86−88% REEs purity) and further purification step will be required in order to divide rare-earth elements. The leach solution can be treated for iron recovery.

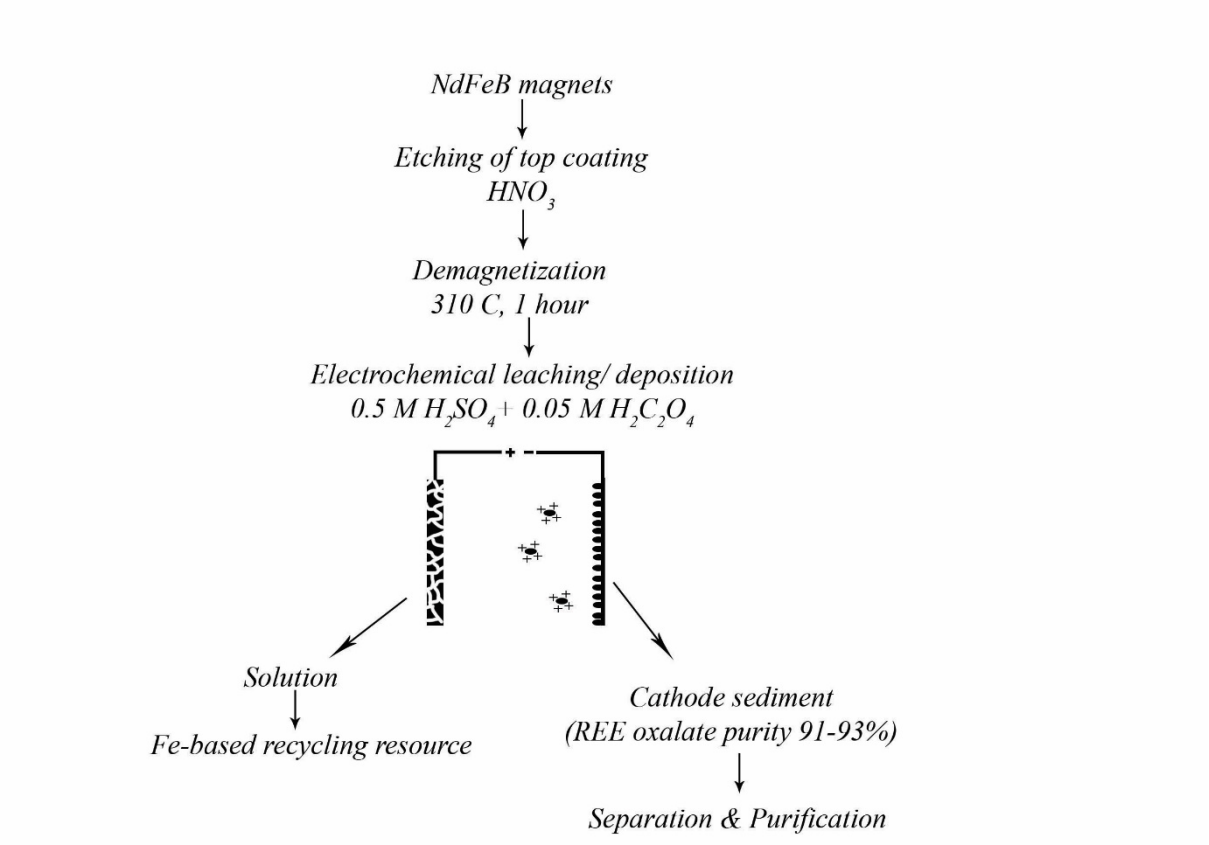

The key finding of this study is deposition of the REEs on the cathode. On thermodynamic basis, direct reduction to a metallic deposit is not possible and the results are explained by electrostatic attraction of the negatively charged REE oxalate particles on the cathode. This possibility has not been mentioned previously for recycling of spent magnets and it may have potential for future recycling methods. Further optimization of the process to increase the REE yield and to minimize energy consumption is currently under investigation in our group.

Acknowledgments

The authors thank the European Regional Development Fund 2014−2020 (project code A74334) for financial support. The authors are grateful to Dr. Liisa Puro and Dr. Toni Väkiparta for their kind support during this project and help in ICP and SEM/EDX measurements; Mohammadamin Esmaelli for his help in zeta potential measurements.

References

1. G. Chauhana, P. R. Jadhaob, K. K. Pantb and K. D. P. Nigam, *J. Environ. Chem, Eng.*, 2018, **6**, 1288–1304.

2. M. T. Islam and N. Huda, *Resour. Conserv. Recycl.*, 2018, **137**, 48–75.

3. J. Feng, F. Zhou, R. Chi, X. Liu, Y. Xu and Q. Liu, *Miner. Eng.*, 2018, **129**, 63–70.

4. A. Battsengel, A. Batnasan, A. Narankhuu, K. Haga, Y. Watanabe and A. Shibayama, *Hydrometallurgy*, 2018, **179**, 100−109.

5. N. A. Mancheri, *Resour. Policy*, 2015, **46**, 262−271.

6. H. Nakamura, *Scr. Mater.*, 2018, **154**, 273−276.

7. J. Gea and Y. Lei, *Resour. Policy*, 2018, 59, 291−297.

8. K. Zhü, S,-Y. Zhao, S. Yang and C. Liang, D. Gu, *Resour. Policy*, 2016, **49**, 349−357.

9. M. Schmid, Resources Policy, Vol. 63, 2019, 101457.

10. D. Yang, S. Gao, J. Hong, L. Ye, X. Ma, C. Qi, X. Li, *J. Waste Manag.*, 2019, **99**, 60−70.

11. K. Hono, H. Sepehri-Amin, *Scr. Mater.*, 2018, **154**, 277−283.

12. J. Ni, W. Luo, C. Hu,Y. Yin, D. Zhang, X. Peng and Q. Han, *J. Magn. Magn. Mater.*, 2018, **468**, 105−108.

13. H. Zeng, Z. Liu, W. Li, J. Zhang, L. Zhao, X. Zhong, H. Yu, B. Guo, *J. Magn. Magn. Mater.*, 2019, **471**, 97−104.

14. J. Li, C. Guo, T. Zhou, Z. Qi, X. Yu, B. Yang and M. Zhu, *J. Magn. Magn. Mater.*, 2018, **454**, 215−220.

15. Y. G. Ma, R. S. Li, Z. Yang, M. Matsumoto, A. Morisako and S.Takei, *Mater. Sci. Eng. B*, 2005, **117**, 287−291.

16. E. Padhan, A. K.Nayak and K. Sarangi, *Hydrometallurgy*, 2017, **174**, 210−215.

17. Y. Tian, Z. Liu and G. Zhang, *J. Rare Earths*, 2019, **37**, 205−210.

18. G. Reisdörfer, D. Bertuol, Eduardo and H. Tanabe, *Miner. Eng.*, 2019, **143**, 105938.

19. C. Tunsu, M. Petranikova, M. Gergorić, C. Ekberg and T.Retegan, *Hydrometallurgy*, 2015, **156**, 239−258.

20. O. Takeda, T. H. Okabe and Y. Umetsu, *J.Alloy Compd.*, 2006, **408–412**, 387–390.

21. Z. Hua, J. Wang, L. Wang, Z. Zhao, X. Li, Y. Xiao and Y. Yang, *ACS Sustainable Chem. Eng.*, 2014, **2**, 2536−2543

22. M. A. R. Önal, C. R. Borra, M. Guo, B. Blanpain and T. V. Gerven, *J. Rare Earths*, 2017, 35, 574.

23. T. V. Hoogerstraete, B. Blanpain, T.V. Gerven and K. Binnemans, *RSC Adv.*, 2014, **4**, 64099-64111.

24. M. Lim and M.J. Kim, *Chemosphere*, 2013, **90**, 1526–1532.

25. F.-L. Mi, S.-J. Wu and F.-M. Lin, *Int. J. Biol. Macromol.*, 2015, **72**, 136–144.

26. P. H. Chen, T. Y. Kuo, F. H. Liu, Y. H. Hwang, M. H. Ho, D. M. Wang, J. Y. Lai and H. J. Hsieh, *J. Agric. Food Chem.*, 2008, **56**, 9015–9021.

27. T. Itakura, R. Sasai and H. Itoh *J.Alloy Compd*, 2006, **408–412**, 1382–1385.

28. P. Venkatesan, Z.H.I. Sun, J. Sietsma and Y. Yang, *Sep. Purif. Technol.* 2017, **191**, 384–391.
29. I. Makarova, E. Soboleva, M. Osipenko, I. Kurilo, M. Laatikainen and E. Repo, *Hydrometallurgy*, 2020, 192, 105264
30. H. Gohr and E. Lange, *Z. Elektrochem.*, 1957, **61**, 1291−1301.
31. A. M. Sukhotin and A. I. Khentov, *Elektrokimia*, 1980, **16**, 1037−1041.
32. Sato, N., Noda, T. and Kudo, K., *Electrochim. Acta*, 1974, **19**, 471−475.
33. A. Kuleyin and H. E. Uysal, *Int. J. Electrochem. Sci.*, 2020, **15**, 1474–1485.
34. J. Fidler and K.G. Knoch, *J. Magn. Magn. Mater.*, 1989, **80**, 48−56.
35. T. Yamashita and P. Hayes, *Appl. Surf. Sci.*, 2008, **254**, 2441–2449.
36. A. P. Grosvenor, B. A. Kobe, M. C. Biesinger and N. S. McIntyre, *Surf. Interface Anal.*, 2004, **36**, 1564 – 1574.
37. A.N. Mansour and R. A. Brizzolara, *Surf. Sci. Spectra*, 1996, **4**, 351.
38. A. N. Mansour and R. A. Brizzolara, *Surf. Sci. Spectra*, 1996, **4**, 345.
39. R. Zhu, Q. Tao, M. Lian, X. Feng, J. Liu, M. Ye, X. Wang, S. Dong, T. Cui and P. Zhu, *Materials* 2019, 12(11), 1780.
40. D. Banerjee, K.J. Sankaran, S. Deshmukh, M. Ficek, C.-J. Yeh, J. Ryl, I-N. Lin, R. Bogdanowickz, A. Kanjilal, K. Haenen and S.S. Roy, *Nanoscale*, 2020.
41. M. Erdemoğlu and M. Sarıkaya, *J. Colloid Interface Sci.*, 2006, **300**, 795−804.
42. E. R. Boevé, L. C. Cao, W. C. D. Bruijn, W. G. Robertson, J. C. Romijn and F. H. Schröder, *J. Urol.*, 1994, **152**, 531−536.

Supplementary

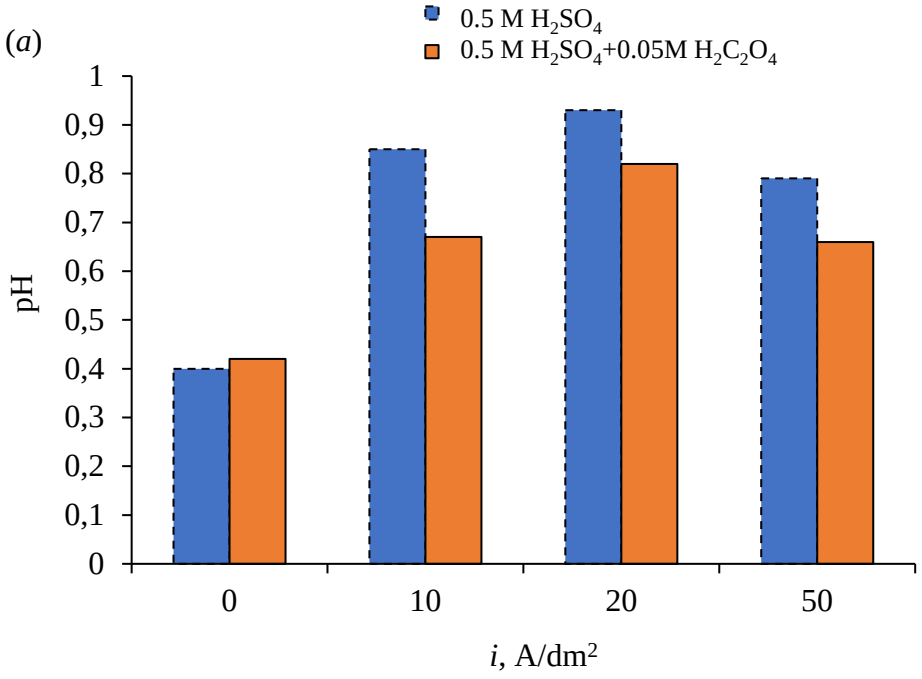

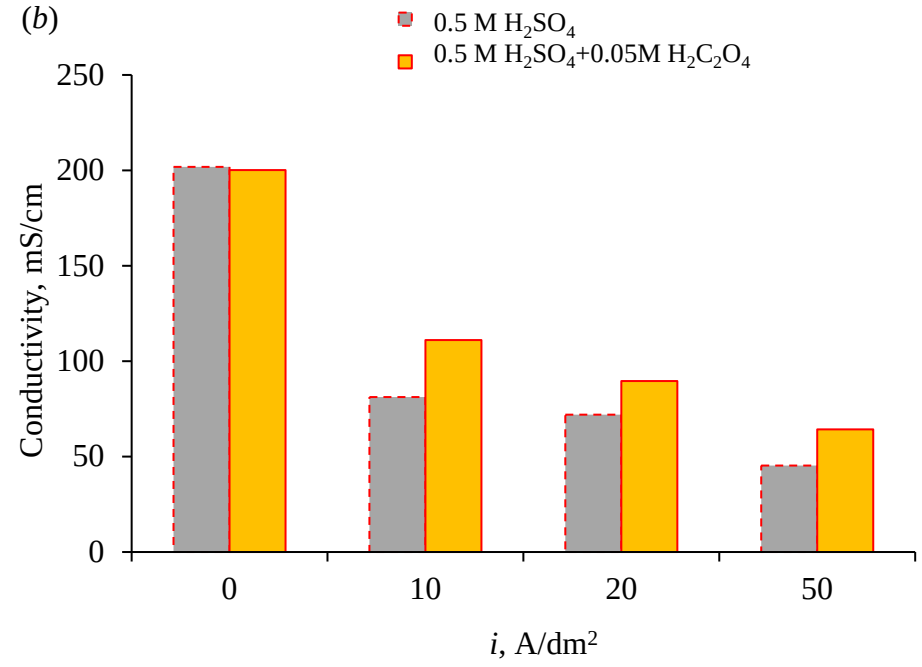

Fig 1S. Effect of current density on pH (*a*) and conductivity (*b*) of solution obtained in H_2SO_4 and mixture of 0.5 M H_2SO_4 and 0.05 M $H_2C_2O_4$ after 1 hour of electrolysis (*i*=0 means initial solution)

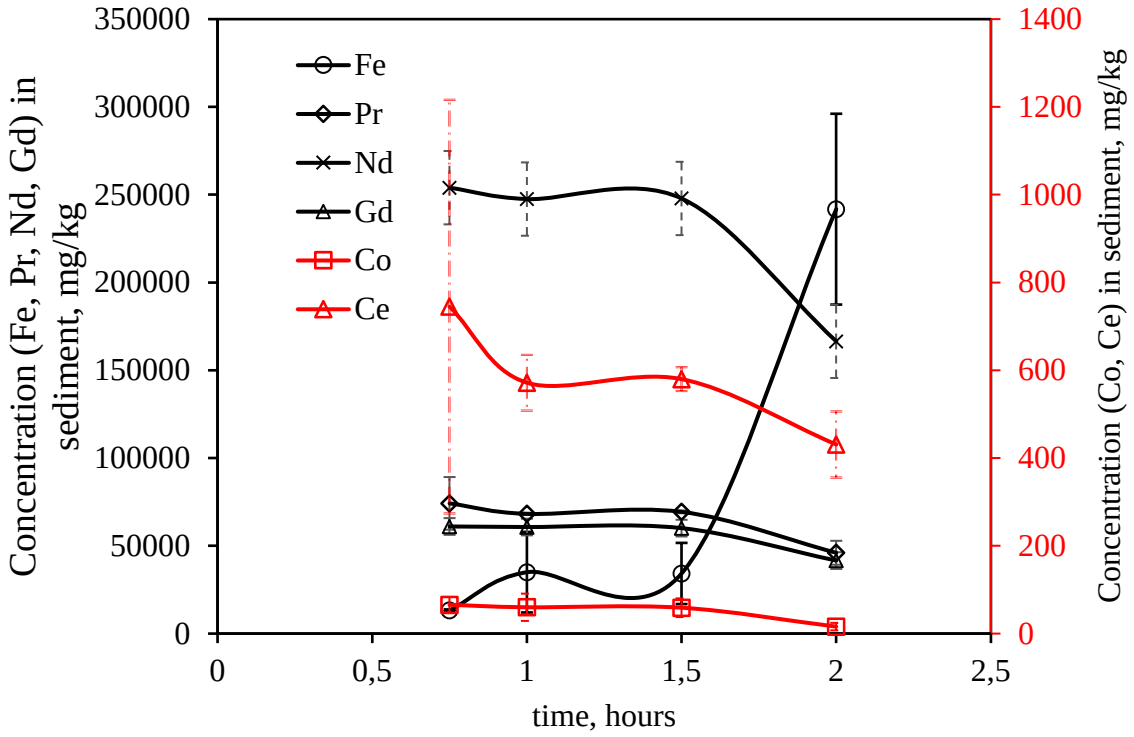

Fig 2S. Effect of time of electrolysis on concentration of Fe and REEs in cathode sediment obtained in mixture of 0.5 M H_2SO_4 and 0.05 M $H_2C_2O_4$ at 50 A·dm^{-2}

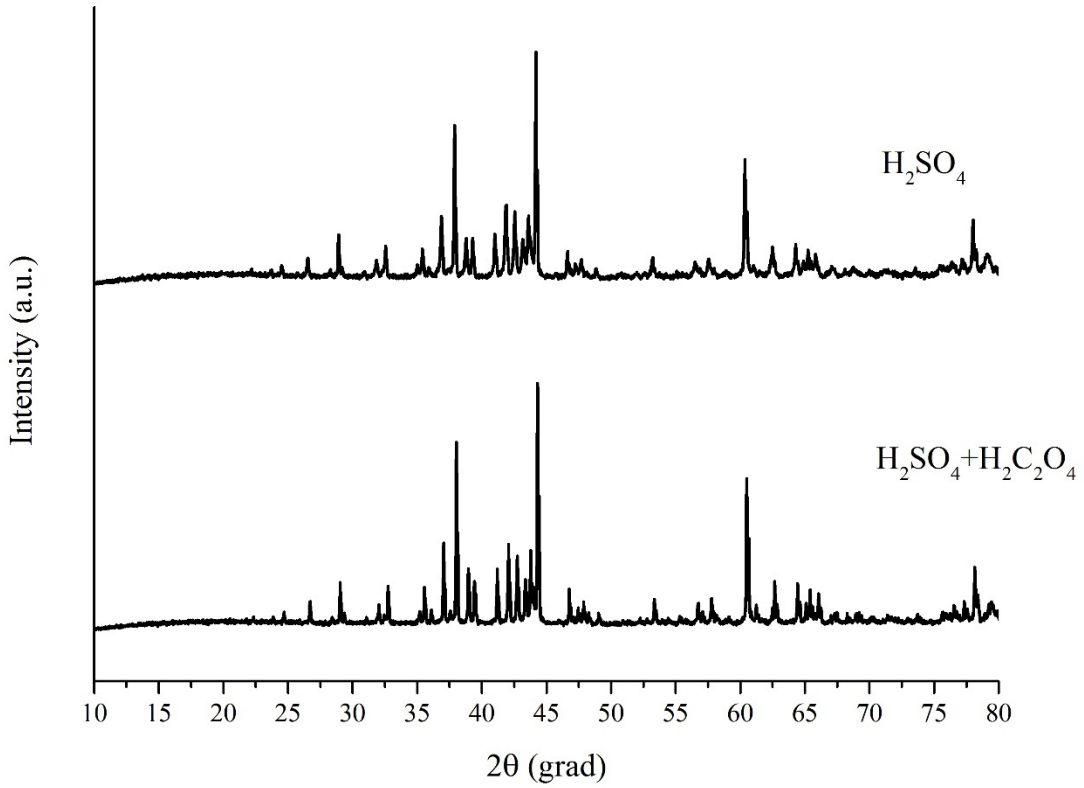

Figure 3S. XRD patterns of NdFeB alloy (original XRD surface [31])

(*a*)

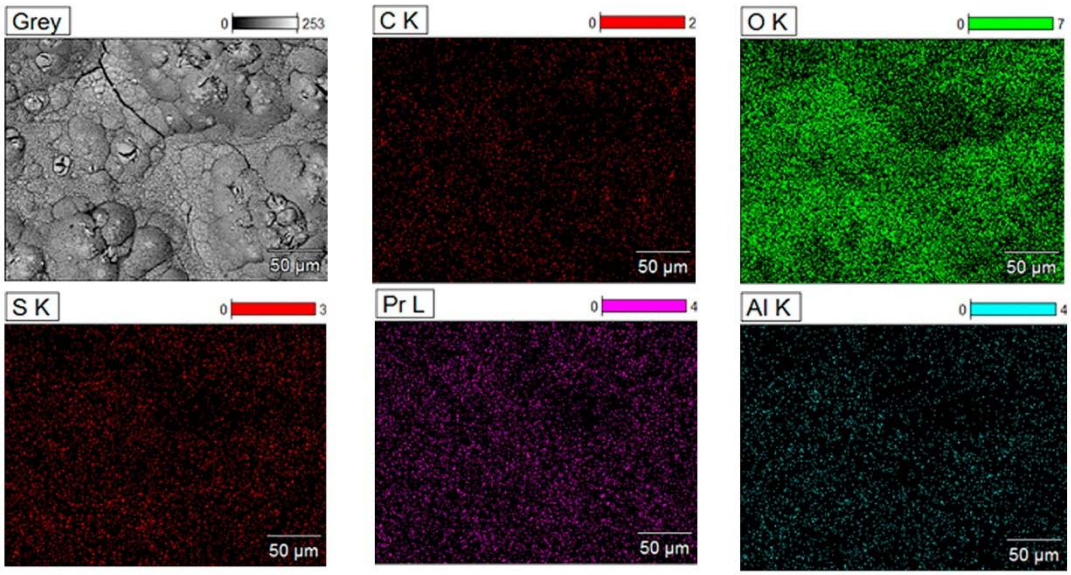

(*b*)

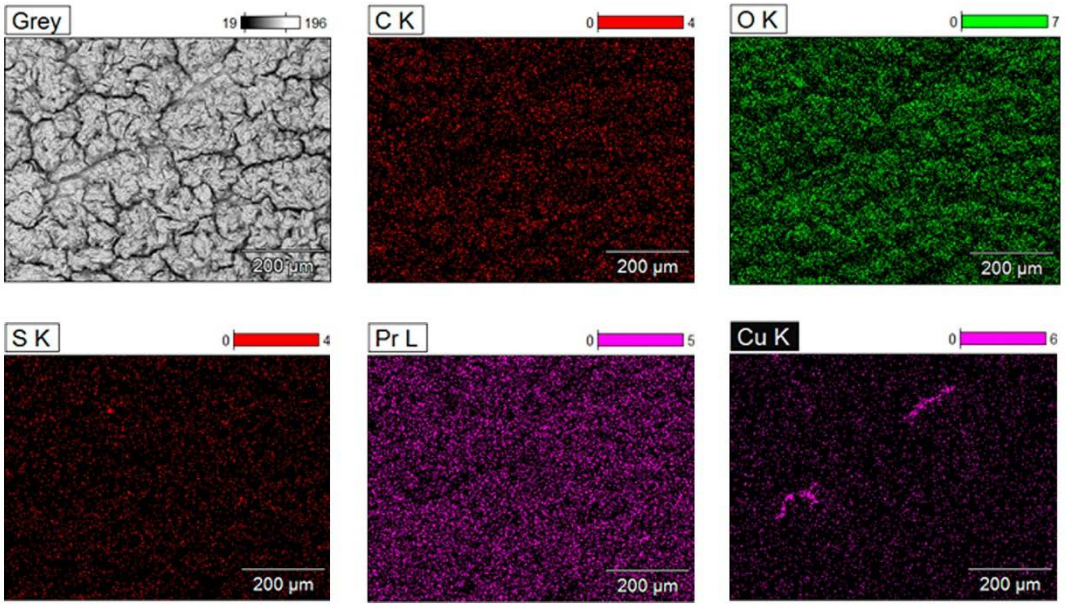

Figure 5S. High-resolution EDX mapping cathodic surface showing different chemical composition after electrolysis, hours: 1 (*a*); 2 (*b*).

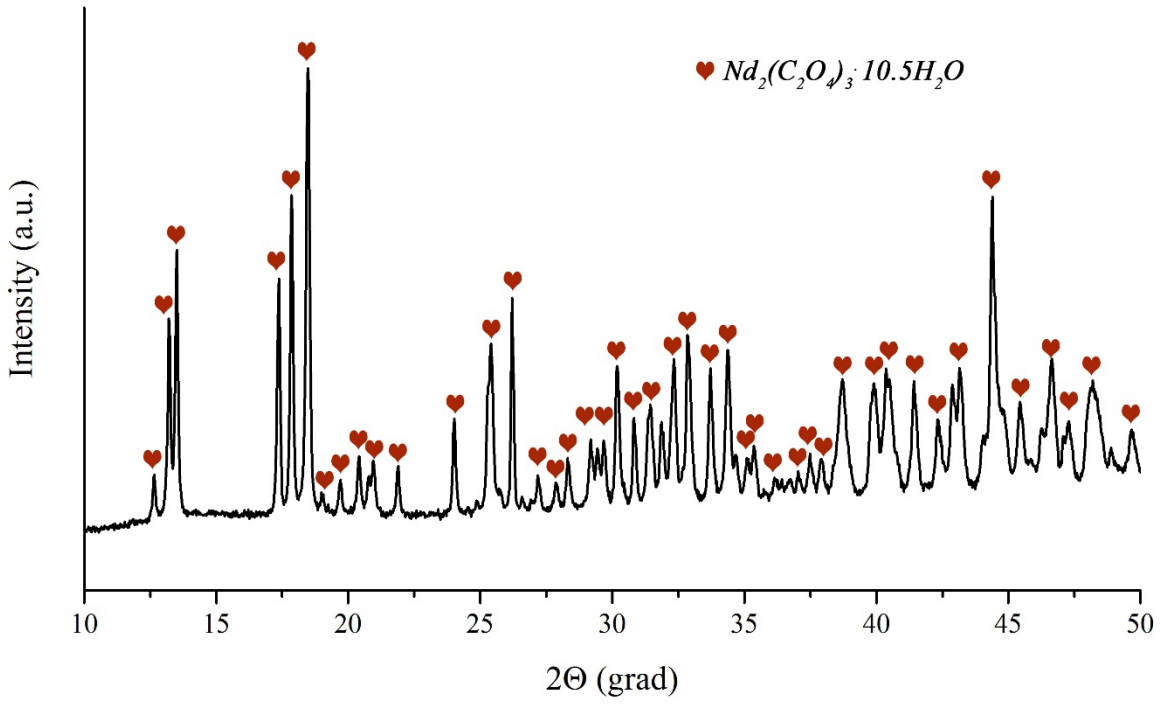

Figure 6S. XRD patterns of a powder obtained after 20 min leaching of spent NdFeB magnet in a mixture of 0.5 M H_2SO_4 and 0.05 M $H_2C_2O_4$ at 50 A/dm^2

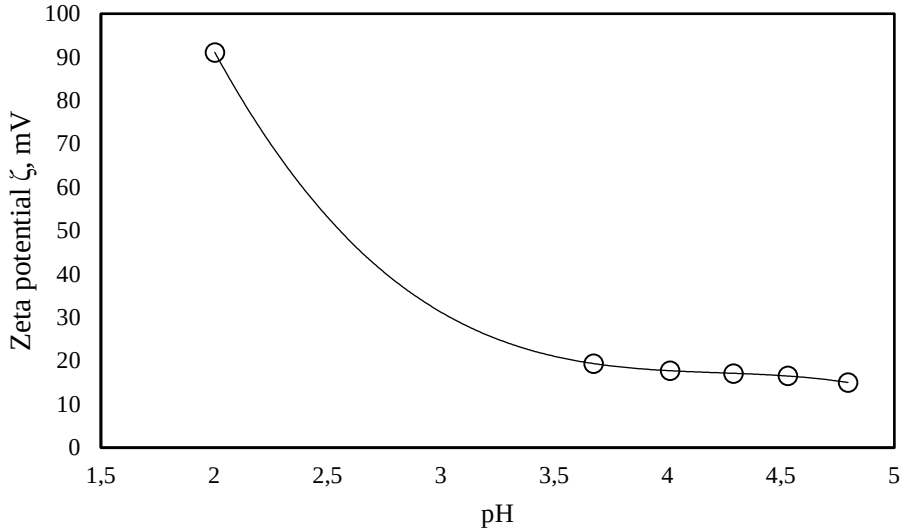

Figure 7S.Zeta potential versus pH for oxalate of neodymium.

Table S1. Equations of cathodic reactions

Equations	Standard potentials, V	
$2Fe^{2+}+3H_2O \rightleftharpoons \gamma Fe_2O_3+6H^+ +2e^-$	E°=0.673	(1)
$2Fe^{2+}+4H_2O \rightleftharpoons Fe_3O_4+8H^+ +2e^-$	E°=0.744	(2)
$2Fe^{2+}+ Fe_3O_4+H_2O \rightleftharpoons \gamma Fe_2O_3+4H^+ +2e^-$	E°=0.592	(3)
$Fe^{2+}+2H_2O \rightleftharpoons Fe(OH)_2+2H^+$	E°=0.65	(4)
$Fe^{3+}+3H_2O \rightleftharpoons Fe(OH)_3+3H^+$	E°=0.61	(5)
$2Fe_3O_4+H_2O \rightleftharpoons 3\gamma Fe_2O_3+2H^+ +2e^-$	E°=0.521	(6)
$\gamma Fe_2O_3+6H_2O \rightleftharpoons \gamma Fe(OH)_3+1.5O_2 +6H^+ +6e^-$	E°=1.241	(7)
$Fe_3O_4+9H_2O \rightleftharpoons Fe(OH)_3+2O_2 +9H^+ +9e^-$	E°=1.171	(8)
$Fe_3O_4+8H^+ \rightleftharpoons 3Fe^{3+}+4H_2O +e^-$	E°=−0.122	(9)
$Fe_3O_4 \rightleftharpoons 3Fe^{3+}+2O_2 +9e^-$	E°=1.13	(10)
$Fe_2O_3 \rightleftharpoons 3Fe^{3+}+1.5O_2 +6e^-$	E°=1.24	(11)

Table S2. EDX analysis of surface of cathodic sediment (wt%) obtained during electro-leaching of NdFeB magnet in 0.5 M H_2SO_4 and 0.05 M $H_2C_2O_4$ at i=50 A/dm^2

	1 hour	1.5 hours	2 hours
C	2.9	11.2	11.2
O	15.0	33.6	27.1
S	0.3	0.4	0.4
Fe	75.4	1.0	0.6
Pr	1.3	9.3	8.6
Nd	4.5	34.0	50.3
Al	0.5	–	–
Gd	–	7.0	–
Cu	–	3.5	1.9